

# CsI-bowl: an ancillary detector for exit channel selection in $\gamma$ -ray spectroscopy experiments\*

Xing-Chi Han,<sup>1,2,†</sup> Shuo Wang,<sup>1,2,†</sup> Hong-Yi Wu,<sup>3</sup> Zhi-Huan Li,<sup>3</sup>  
Guo-Zhu Shi,<sup>4</sup> Ruo-Fu Chen,<sup>4</sup> Yue-Zhao Zhang,<sup>1,2</sup> and Shou-Yu Wang<sup>1,2</sup>

<sup>1</sup>Shandong Provincial Key Laboratory of Optical Astronomy and Solar-Terrestrial Environment,

School of Space Science and Physics, Institute of Space Sciences, Shandong University, Weihai, 264209, China

<sup>2</sup>WeiHai Research Institute of Industrial Technology of Shandong University, Weihai 264209, People's Republic of China

<sup>3</sup>School of Physics and State Key Laboratory of Nuclear Physics and Technology, Peking University, Beijing 100871, China

<sup>4</sup>Institute of Modern Physics, Chinese Academy of Sciences, Lanzhou, 73000, People's Republic of China

A particle detector array designed for light-charged particles, known as the CsI-bowl, was built for exit channel selection for in-beam  $\gamma$ -ray spectroscopy experiments. This device is composed of 64 CsI(Tl) detectors, organized in a structure reminiscent of a tea-bowl. High quantum efficiency photodiodes, characterized by their minimal mass, were employed to collect scintillation light. Its design, construction, particle identification resolution, and its effectiveness in relation to exit channel selection is described in this paper. In source tests, the optimal figure of merit for the identification of  $\alpha$ -particles and  $\gamma$ -rays using the charge comparison method was found to be 3.3 and 12.1 for CsI detectors coupled to photodiodes and avalanche photodiodes, respectively. The CsI-bowl demonstrated effectiveness in identifying particles, specifically the emission of protons and  $\alpha$ -particles in the  $^{58}\text{Ni}(^{19}\text{F}, xpyn)$  fusion–evaporation reaction, thereby enabling the selection of the desired exit channels.

Keywords: Light charged particle detector array, Particle identification, Charge comparison method

## I. INTRODUCTION

For many decades, high-resolution  $\gamma$ -ray spectroscopy, facilitated by large HPGe detector arrays, such as GAMMA-SPHERE [1] and EUROBALL [2], has been instrumental in accumulating extensive knowledge about nuclear behavior at high spins and excitations. This method has served as a fundamental element in the study of nuclear structures [3]. The fusion–evaporation reaction induced by heavy-ions is the most effective method to maintain a balance between high angular momentum and a large cross-section. However, this reaction populates a considerable number of exit channels, which complicates the selection of a specific channel for investigation. As a typical solution, data analysis often involves the use of  $\gamma$ -ray multiplicity gating techniques.

However, for nuclei of medium or low atomic number ( $A$ ), the large cross sections for charged particle emissions result in numerous channels with comparable  $\gamma$ -ray multiplicities. These channels cannot be separated by employing  $\gamma$ -ray multiplicity gating alone. In these instances, conducting measurements for the simultaneous emission of protons,  $\alpha$ -particles, and  $\gamma$ -rays in the fusion–evaporation reaction can enhance the selection of the channel of interest. Hence, a light-charged particle detector array is commonly used as an auxiliary detector to enhance the peak-to-background ratio in  $\gamma$ -ray spectroscopy, as observed in examples like Microball [4] and DIAMANT [5]. These two ancillary detectors were composed of CsI(Tl) scintillators, which exhibit several advantages over silicon detectors, including low cost, ease of machining, and strong resistance to radiation.

The advent of high-speed analog-to-digital converters (ADCs) with excellent electronic resolution has catalyzed novel opportunities for digital processing of pulses from detectors, simplifying the configuration of readout electronics [6]. Leveraging these benefits, digital data acquisition systems have become increasingly prevalent in recent years, surpassing traditional analog data acquisition systems in the realm of nuclear physics research [7, 8].

When comparing pulse shape discrimination (PSD) [9] with the traditional analog electronics used in microballs and DIAMANT, it was observed that the capability of particle identification (PID) with a digital data acquisition system can be further improved via pulse shape analysis (PSA) of the stored waveforms [10].

Recently, research interest has significantly increased in the study of nuclei with  $A \approx 80$ , owing to the presence of numerous intriguing nuclear structure phenomena, such as multiple chiral doublet bands with octupole correlations. For a detailed study of this mass region, a light-charged particle detector array, termed as the CsI-bowl, with a digital data acquisition system was constructed at Shandong University (Weihai) for  $\gamma$ -ray spectroscopy experiments. The following section outlines the technical layout of the proposed array. Section II describes the design and construction of the CsI-bowl. In Section III, the PID resolutions of CsI-PD and CsI-APD detectors in the source tests are presented using charge comparison and waveform fitting methods. The results of the channel-selection performance in the  $^{58}\text{Ni}(^{19}\text{F}, xpyn)$  reaction with the AFRODITE array at iThemba LABS are shown.

## II. DETECTOR CONFIGURATION

To select the exit channels of interest in the fusion–evaporation reaction, the light-charged particle detector array should satisfy the following criteria: (i) good PID reso-

\* Supported by the Major program of Natural Science Foundation of Shandong Province (Grant No. ZR2020ZD30), the National Natural Science Foundation of China (Grant Nos. 11775133, U2167202, U1432119).

† Corresponding author, wangshuo\_wh@sdu.edu.cn

lution for light-charged particles, especially for protons and  $\alpha$ -particles; (ii) large solid-angle coverage; (iii) minimum absorption and scattering for  $\gamma$ -rays; (iv) reasonable granularity to reduce the probability of multiple hits in one detector; (v) good resistance to radiation damage; and (vi) small size

For the detection of charged particles, scintillators, such as NaI(Tl) [11–13], CsI(Tl) [9, 14, 15], and LaBr<sub>3</sub> [16–18], are undoubtedly some of the most frequently and widely used in nuclear and particle physics experiments. The overall decay time of the emitted light pulse in certain scintillators will vary with the type of exciting radiation and such scintillators are thus capable of pulse shape discrimination. The CsI(Tl) scintillator is known to exhibit a predominantly two-component scintillation process, with a fast component having decay times of  $\tau_f = 0.4 \sim 1.0 \mu\text{s}$  and a slow component having decay times of  $\tau_s = 7.0 \mu\text{s}$  [4]. The relative populations of the two components depend on the type of ionizing radiation [19, 20]. In general, the fast decay time  $\tau_f$  increases as the ionization density of the detected particle decreases, whereas the ratio between the fast and slow components decreases. Additionally, the high conversion efficiency of the CsI(Tl) scintillator (64000 photons / MeV) results in signals with high signal-to-noise ratios, which can lead to good PID resolution [21]. Thus, the CsI(Tl) scintillator has been chosen as the detector material.

Considering the geometric structure, the assembly of the AFRODITE array, absorption of the  $\gamma$ -rays, and size of the CsI(Tl) crystals were chosen as  $10 \times 10 \times 5 \text{ mm}^3$ , and the maximum energy deposited in those crystals was 35 MeV for protons and 130 MeV for  $\alpha$ -particles. This is enough sufficient for depositing the emission-charged particles in fusion-evaporation reaction. The crystals were produced at the Institute of Modern Physics at the Chinese Academy of Sciences (IMPCAS) [22]. The scintillation light was collected using a the Hamamatsu S3590 PIN photodiode (PD) or S8664-1010 avalanche photodiodes (APD) with a photosensitive areas of  $10 \times 10 \text{ mm}^2$ . The crystals were coupled to the PDs or APDs using light guided silicone grease (EJ-550), and special care was taken to ensure that the silicone grease was free of bubbles, typically by pressing and sliding to squeeze out the bubbles. Each crystal was placed into a SiO<sub>2</sub> container, which served as a reflector for the scintillation light and provided a compact CsI-PD or CsI-APD assembly. The face of the crystal was covered with aluminized Mylar foil of  $2.0 \mu\text{m}$  to improve light collection. All CsI(Tl) detectors were soldered onto a PCB substrate via two brass pins of PDs or APDs, and the signals were sent to a compact 16-channel integrated charge sensitive preamplifier MODEL SPA02-16 [23]. The preamplifiers were designed and manufactured by the China Institute of Atomic Energy (CIAE).

### III. PERFORMANCE OF THE DETECTOR ARRAY

The capability of PID for each CsI(Tl) detector was determined by  $\gamma$ -source  $^{60}\text{Co}$  and  $\alpha$ -source ( $^{241}\text{Am}$  and  $^{239}\text{Pu}$  mixed) a schematic view of the experimental setup is shown in Fig. 1. The channel-selection performance of the CsI-

bowl was examined in the  $^{58}\text{Ni}(^{19}\text{F}, xpy_n)$  reaction with the AFRODITE array at iThemba LABS. During the experiments, the waveforms were recorded and saved on a computer using XIA Pixle-16 modules from XIA LLC [24]. Offline digital signal processing was performed based on the ROOT data analysis framework [25].

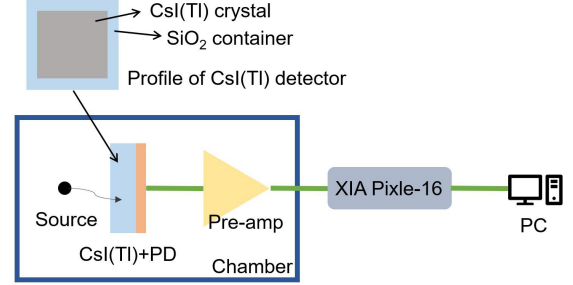


Fig. 1. (Color online) Schematic view of the experimental set-up using  $\gamma$ -source and  $\alpha$ -source.

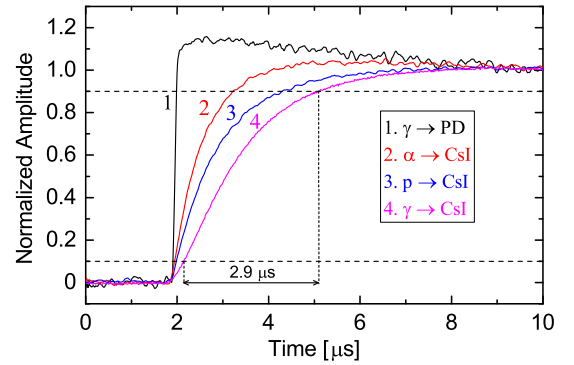


Fig. 2. (Color online) Sample waveforms show different pulse shapes due to protons,  $\alpha$ -particles and  $\gamma$ -rays impinging on the CsI(Tl) crystal, and the fast rise-time trace (labeled 1) is from  $\gamma$ -ray interaction directly on the silicon photodiode. To facilitate the comparison, the waveforms were normalized to the same height at  $t = 10 \mu\text{s}$  and their baselines were shift to zero.

#### A. PID resolution of the detector

Figure 2 shows four types of sample waveforms after amplitude normalization and baseline subtraction: 1) photon conversion directly in the PD, 2)  $\alpha$ -particles impinging on the CsI(Tl) crystal, 3) protons impinging on the CsI(Tl) crystal, and 4)  $\gamma$ -rays impinging on the CsI(Tl) crystal. The rise time (from 10% to 90% peak amplitude) of these waveforms are approximately 0.08, 1.2, 2.3, and  $2.9 \mu\text{s}$ , respectively. According to the different rise times of the waveforms, the PID resolution was examined using the charge comparison [26, 27] and waveform fitting methods [28, 29]. The charge comparison method is based on an analysis of the relative population of fast and slow decay components to dis-

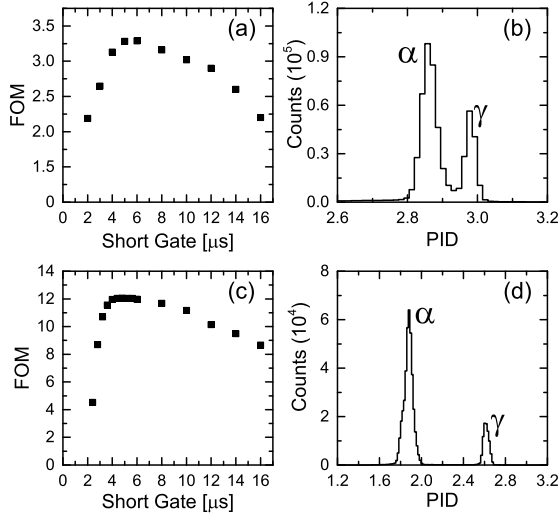


Fig. 3. For  $\alpha$ -particles and  $\gamma$ -rays, the FOM values change as a function of short gate interval for (a) CsI-PD detector and (c) CsI-APD detector and the PID spectra were obtained using the charge comparison method for (b) CsI-PD detector and (d) CsI-APD detector.

tinguish different types of particles by integrating a shorter window near the peak ( $Q_{short}$ ) and longer window encompassing the majority of the waveform ( $Q_{long}$ ). In the source tests, different integral intervals were employed for the analysis of the waveforms to determine the optimal parameters for the in-beam experiments. The PID resolution of a detector is usually quantified using the figure of merit (FOM) [30, 31] defined as

$$FOM = \frac{|\mu_\alpha - \mu_\gamma|}{FWHM_\alpha + FWHM_\gamma} \quad (1)$$

where  $\mu$  and FWHM denote the centroids and full-width-at-half-maximum of the  $\alpha$ - and  $\gamma$ -ray peaks, respectively. Give that the FOM values are not sensitive to the  $Q_{long}$  value [30], only a short gate interval is adjusted to optimize the PID resolution. Figure 3 (a) shows the FOM values with different short gate integrals for the CsI-PD detector; the optimal value of FOM is obtained as 3.3 with a short gate interval of approximately 5  $\mu$ s. For the comparison of PID resolution, a PID parameter is usually set as the ratio of  $Q_{long}$  to  $Q_{short}$ , and the PID spectrum at FOM = 3.3 is shown in Fig. 3(b) to distinguish  $\alpha$ -particle and  $\gamma$ -ray. Owing to the internal gain (50–100) of APD, the PID resolution of CsI-APD detector is significantly improved with a high signal-to-noise ratio, and

the optimal value of FOM obtained is 12.1 with a short gate interval of approximately 4.0  $\mu$ s, as shown in Fig. 3 (c) and (d).

In the waveform fitting method, the light output of the CsI(Tl) scintillator can be modeled using a combination of two exponential functions with fast and slow decay time constants [32]:

$$L(t) = \frac{N_f}{\tau_f} e^{-\frac{t}{\tau_f}} + \frac{N_s}{\tau_s} e^{-\frac{t}{\tau_s}} \quad (2)$$

$$G(t) = A e^{-t/\tau_p} \quad (3)$$

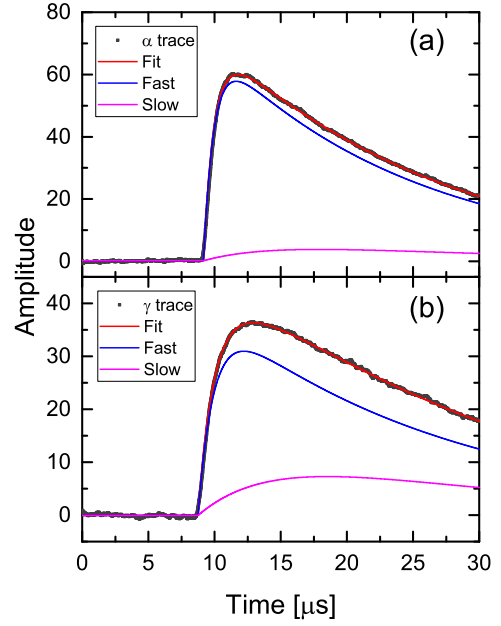


Fig. 4. (Color online) Experimental baseline subtraction waveforms (black dash) and the least square fit results (red line) of (a)  $\alpha$ -particle and (b)  $\gamma$ -ray. The blue and magenta lines illustrate the fast and slow components of the signal, respectively.

where  $L(t)$  denotes the light pulse amplitude at time  $t$ ;  $\tau_f$  and  $\tau_s$  denote the decay time constants for the fast and slow components, respectively, with amplitudes  $N_f$  and  $N_s$ . The preamplifier output signal  $U(t)$  is described by the convolution between the light output function,  $L(t)$  and preamplifier impulse response function,  $G(t)$ , an exponential function with a decay time constant  $\tau_p$ . The functional form of the signal  $U(t)$  is obtained via Eq. 4 for the times before and after the beginning of the signal at  $t_0$ .

$$U(t) = \int_0^t L(t') G(t-t') dt' = \begin{cases} C & t < t_0 \\ C + \frac{N_f \tau_p}{\tau_p - \tau_f} \left[ e^{-\frac{t-t_0}{\tau_p}} - e^{-\frac{t-t_0}{\tau_f}} \right] + \frac{N_s \tau_p}{\tau_p - \tau_s} \left[ e^{-\frac{t-t_0}{\tau_p}} - e^{-\frac{t-t_0}{\tau_s}} \right] & t \geq t_0 \end{cases} \quad (4)$$

where constant  $C$  denotes the baseline of the signal. The relative intensities of the fast and slow components depend on the stopping power  $dE/dx$  of the particle in the detector. A higher ionization loss produces a higher density of free electrons and holes, leading to a faster component.

To accelerate the fitting procedure and improve the fitting accuracy, it is necessary to reduce the number of free parameters and provide suitable initial values. The baseline constant  $C$ , which is determined from the average value of the samples proceeding to the leading edge, is set to a fixed value for each waveform. In the fitting processes, the parameter  $\tau_p$  is set to  $15.4 \mu\text{s}$ . This value is determined by performing a large number of fittings of the pulse tails (ranging from 20 to  $30 \mu\text{s}$ ) using a single exponential decay function  $G(t)$ . The fast decay constant  $\tau_f$  was limited from 0.4 to  $1.0 \mu\text{s}$ , and the slow decay constant  $\tau_s$  was fixed at  $7.0 \mu\text{s}$ , as mentioned above. The other four parameters ( $t_0, \tau_f, N_f$  and  $N_s$ ) are determined by applying a least squares fit to the waveform. A linear fit to the beginning of the leading edge is implemented to obtain the initial value  $t_0$ . The intersection between the fitting function and baseline can be calculated to obtain the value  $t_0$ , where the signal begins to rise. The initial value  $\tau_f = 0.7 \mu\text{s}$  was set as the central value for the limited range of  $0.4\text{--}1.0 \mu\text{s}$ . Meanwhile,  $N_f$  and  $N_s$  are initially set to half the amplitude of the waveform. The fitting results for  $\alpha$ -particle and  $\gamma$ -ray waveforms obtained using the analytical function Eq. 3 are shown in Fig. 4 (a) and (b). The fast and slow components can be clearly obtained, and the proportions of the fast and slow components are obviously different for  $\alpha$ -particle and  $\gamma$ -ray. Thus, the PID for different types of incident particles can be obtained from the ratios of the fast and slow components of the waveforms. Figure 5 shows the optimal two-dimensional PID spectra for the CsI-PD and CsI-APD detectors using charge comparison and waveform fitting methods. The  $\alpha$ -particles and  $\gamma$ -rays were clearly separated by both methods, whereas the PID capability could be slightly improved by the waveform fitting method when compared to that by the charge comparison method. However, the fitting method requires the storage of the entire waveform, which results in high memory consumption during the experiments. Therefore, the charge comparison method was employed to obtain PID information in the in-beam experiment, and the integral values of  $Q_{\text{short}}$  and  $Q_{\text{long}}$  were recorded. Although the PID capability of CsI-APD detector is better than that of CsI-PD detector, the CsI-PD detector applicable for the in-beam experiments due to the disadvantage of the gain instability with respect to the temperature of APD [33].

### B. In-beam performance of the CsI-bowl

The CsI-bowl was paired with the AFRODITE array [34] at iThemba LABS as a channel selection device during the  $^{58}\text{Ni}(^{19}\text{F}, xpy)n$  in-beam  $\gamma$ -spectroscopy experiment. This setup can cover the angular range from  $35^\circ$  to  $85^\circ$  downstream, and from  $143^\circ$  to  $155^\circ$  upstream, as depicted in Fig. 6. The  $^{19}\text{F}$  ions with an energy of 62 MeV were used to bombard a target comprising  $1.0 \text{ mg/cm}^2$  of highly enriched  $^{58}\text{Ni}$

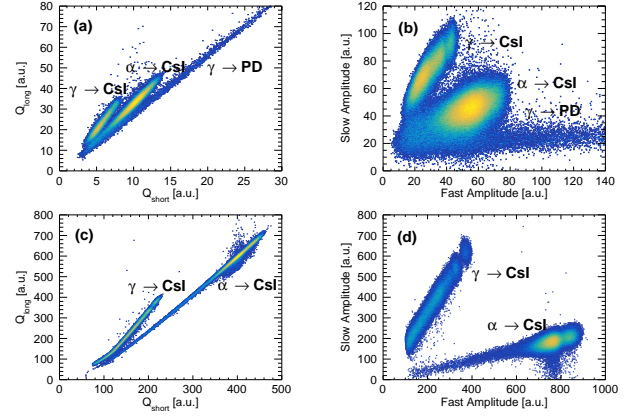


Fig. 5. (Color online) Particle identification plots for  $\alpha$ -particles and  $\gamma$ -rays in the source tests using the charge comparison method and waveform fit method, (a) and (b) for the CsI(Tl)-PD detector and (c) and (d) for the CsI(Tl)-APD detector. All units in the figure correspond to arbitrary units.

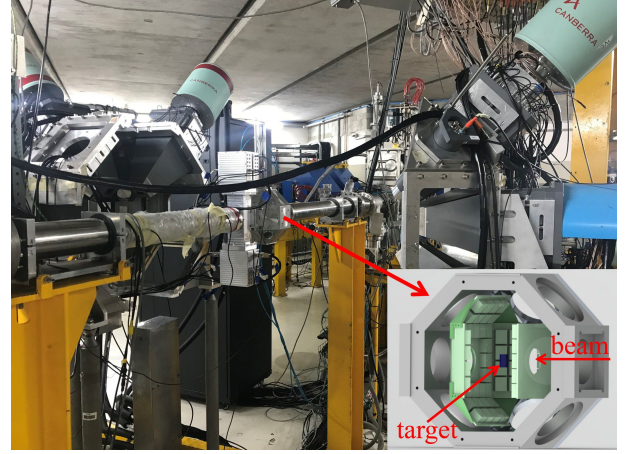


Fig. 6. (Color online) CsI-bowl inside the reaction chamber coupled with the AFRODITE array at the iThemba LABS. The inset shows the schematic drawing of the CsI-bowl, and  $^{58}\text{Ni}$  target was placed in the center of the chamber.

evaporated onto a  $12.8 \text{ mg/cm}^2$  Au backing. Throughout the fusion-evaporation reaction, several nuclei in excited states were produced, such as  $(1\alpha 3p)^{70}\text{Ge}$ ,  $(1\alpha 2p)^{71}\text{As}$ ,  $(\alpha p)^{72}\text{Se}$ ,  $(3p)^{74}\text{Se}$ ,  $(2p 1n)^{74}\text{Br}$ , and  $(1p 1n)^{75}\text{Kr}$ . The energy regions of the emission protons and  $\alpha$ -particles were approximately 3–18 MeV and 7–24 MeV, respectively. The  $\gamma$ -rays from the decay of the excited nuclear states were recorded by the eight Compton-suppressed Clover detectors, while charged particles were detected by the CsI-bowl. Particle and  $\gamma$ -ray coincidence events were selected by applying a 300-ns time-window.

The two-dimensional PID histogram obtained using the charge comparison method and PID resolution plot of the CsI-bowl are shown in Fig. 7 (a) and (b), and approximately 93% of the detected light-charged particles can be distinguished as protons and  $\alpha$ -particles. The exit channels of interest can be



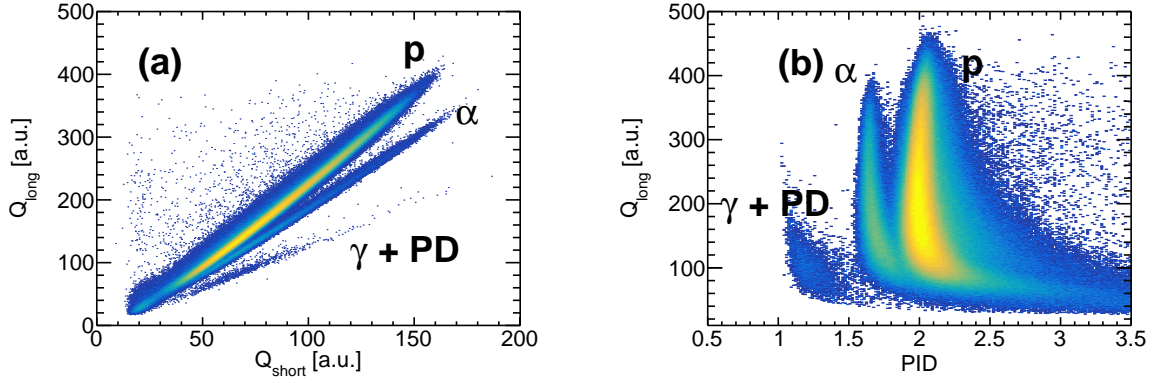


Fig. 7. (Color online) PID resolution for protons and  $\alpha$ -particles of the CsI-bowl using the charge comparison method in the  $^{58}\text{Ni}(^{19}\text{F}, x\text{pyn})$  fusion–evaporation reaction. (a) Plot of  $Q_{\text{long}}$  with respect to  $Q_{\text{short}}$ . (b) Plot of PID parameter with respect to  $Q_{\text{long}}$  value. The PID parameter is obtained by the ratio of  $Q_{\text{long}}$  and  $Q_{\text{short}}$ .

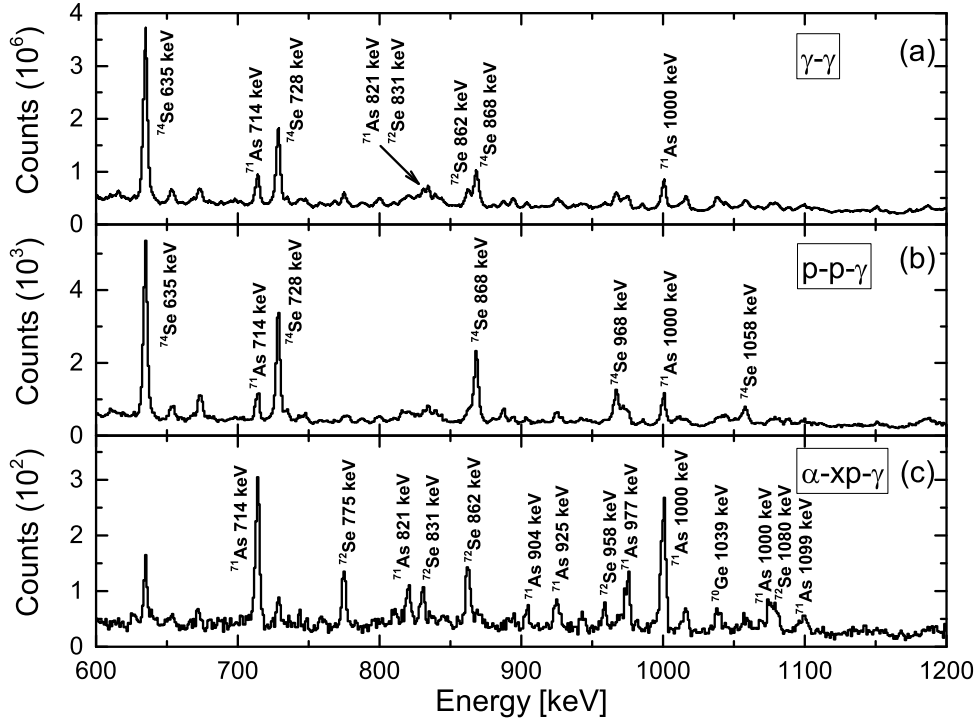


Fig. 8. Gamma-ray spectra from the reaction of  $^{58}\text{Ni}(^{19}\text{F}, x\text{pyn})$  with beam energy 65 MeV. (a) Total  $\gamma$ - $\gamma$  projection spectrum, (b)  $\gamma$ -ray spectrum for two protons emission channels and (c)  $\gamma$ -ray spectrum for  $\alpha$ -xp emission channels.

selected by gating different numbers of  $\alpha$ -particles and protons. The  $\gamma$ - $\gamma$  coincidence spectrum of the  $^{58}\text{Ni}(^{19}\text{F}, x\text{pyn})$  reaction is shown in Fig. 8 (a). The prominent peaks in the spectra at 635, 728, 868, 714, and 1000 keV stem from  $^{74}\text{Se}$  and  $^{71}\text{As}$ . Based on calculations using the PACE4 [35, 36] computer code, these nuclei are the frequent product of evaporation of  $^{19}\text{F}$  with  $^{58}\text{Ni}$ . The  $\gamma$ -ray spectrum gated to two protons is shown in Fig. 8(b). The yrast  $\gamma$ -ray transitions of  $^{74}\text{Se}$  under  $10^+$  were strongly enhanced, and almost all con-

taminations from other exit channels were eliminated. The  $\gamma$ -ray spectrum in coincidence with one  $\alpha$ -particle and  $x$  protons, achieved with PID gates, is shown in Fig. 8 (c), and the  $\gamma$ -rays of  $^{71}\text{As}$ ,  $^{72}\text{Se}$  and  $^{70}\text{Ge}$  are clearly enhanced with respect to the channels without  $\alpha$ -particle emission. Furthermore, it is an effective way to distinguish similar energies of  $\gamma$ -rays from different exit channels using light-charged particle gating technique. As shown in Fig. 8 (a), the 862 keV  $\gamma$  transition from  $2^+$  to  $0^+$  of the yrast states in  $^{72}\text{Se}$  [37] is

mixed with the 868 keV  $\gamma$  transitions from  $6^+$  to  $4^+$  of the yrast states in  $^{74}\text{Se}$  [38]. The exit channel of  $^{72}\text{Se}$  is populated with one  $\alpha$ -particle and one proton emission from the compound nucleus, whereas the exit channel of  $^{74}\text{Se}$  has three proton emissions. The 862 keV  $\gamma$  transition from  $^{72}\text{Se}$  can be completely eliminated by gating the two protons, as shown in Fig. 8(b), and the 868 keV  $\gamma$  transition from  $^{74}\text{Se}$  disappeared by gating one  $\alpha$ -particle and  $x$  protons, as shown in Fig. 8(c). Another advantage of exit-channel selection is the enhancement of weak  $\gamma$  transitions against the background. As shown in Fig. 8 (a), the 821 and 831 keV  $\gamma$  transitions in  $^{71}\text{As}$  and  $^{72}\text{Se}$  cannot be discriminated using only the  $\gamma$ - $\gamma$  coincidence spectrum because of the strong  $\gamma$ -ray background from other channels. After  $\alpha$ - $xp$ - $\gamma$  coincidence gating, the two  $\gamma$  transitions can be clearly distinguished, as shown in Fig. 8(c). Consequently, these results provide unambiguous verification of the capability of the CsI-bowl as a channel-selection device.

#### IV. SUMMARY AND OUTLOOK

The CsI-bowl is designed, constructed, and commissioned as an ancillary detector for in-beam  $\gamma$ -spectroscopy experiments to provide select the exit channels. The particle identification resolutions of the CsI coupled with photodiode and avalanche photodiode detectors were studied using  $\gamma$ -source  $^{60}\text{Co}$  and  $\alpha$ -source ( $^{241}\text{Am}$  and  $^{239}\text{Pu}$  mixed) via the charge-comparison and waveform fitting methods. The optimal value of the figure of merit for distinguishing  $\alpha$ -particles and  $\gamma$ -rays was found to be 3.3 using the charge comparison method for CsI coupled with photodiode detectors, and the optimal value of the figure of merit was equal to 12.1 for the CsI coupled with avalanche photodiode detectors, due to the internal gain of avalanche photodiode. The particle identification resolution can be slightly improved via the fit waveform method when compared to that obtained via the charge comparison method. In the  $^{58}\text{Ni}(^{19}\text{F}, xp\gamma n)$  experiment, approximately 93% of the protons and  $\alpha$ -particles were clearly identified, and the capability of the CsI-bowl as a channel selection device was determined. The present measurements highlight the improved sensitivity of  $\gamma$ -ray spectroscopy using the CsI-bowl coupled with an AFRODITE array.

With the development of the new scintillation materials  $\text{LaBr}_3(\text{Ce})$  and  $\text{CeBr}_3$  [39] in the last decade, hybrid  $\text{LaBr}_3(\text{Ce})$ -HPGe arrays [40, 41] have become mainstream detection arrays in nuclear spectroscopy experiments for the measurement of excited nuclear state lifetimes [42–44], providing essential insights into the structure of nuclei. A hybrid  $\text{CeBr}_3/\text{LaBr}_3(\text{Ce})$ -HPGe array is currently under construction for nuclear structure studies at Shandong University (Weihai). The hybrid  $\text{CeBr}_3/\text{LaBr}_3(\text{Ce})$ -HPGe array allows the installation of up to 10 HPGe and 16  $\text{CeBr}_3/\text{LaBr}_3(\text{Ce})$  detectors. An updated version of the CsI-ball, which has nearly  $4\pi$  solid angle coverage, as an ancillary detector for the hybrid  $\text{CeBr}_3/\text{LaBr}_3(\text{Ce})$ -HPGe array is also under construction. The scintillation light is collected by silicon photomultiplier [45, 46] to further improve the particle identification capabilities. With the high gain ( $10^5$ – $10^7$ ) of silicon photo-

multiplier, the waveform of signals can be recorded directly via the digital data acquisition system without the preamplifier. The length of the waveform is approximately  $3\ \mu\text{s}$ , which allows the entire waveform to be recorded at a high counting rate during the experiment. Owing to the strong function of the gain and temperature of the silicon photomultiplier, a temperature-compensated bias voltage system has already been developed, and the bias voltage is precisely controlled using a thermosensor to maintain a constant gain during the experiment.

#### V. ACKNOWLEDGMENTS

The exceptional skill demonstrated by the staff from the Crystal Group at IMPCAS during the construction of the CsI-bowl, as well as the outstanding collaboration with Nuclear Reaction Group from the China Institute of Atomic Energy during preamplifier testing, is greatly appreciated. The authors also extend their gratitude towards the technical staff and accelerator group at iThemba LABS for their consistent support throughout the experiment.

- [1] L.Y. Lee, The gammasphere. Nucl. Phys. A **520**, c641-c655 (1990). [https://doi.org/10.1016/0375-9474\(90\)91181-P](https://doi.org/10.1016/0375-9474(90)91181-P)
- [2] J. Simpson, The euroball spectrometer. Z. Phys. A **358**, 139-143 (1997). <https://doi.org/10.1007/s002180050290>
- [3] S. Akkoyun, A. Algora, B. Alikhani et al., AGATA — advanced gamma tracking array. Nucl. Instrum. Methods Phys. A **668**, 26-58 (2012). <https://doi.org/10.1016/j.nima.2011.11.081>
- [4] D.G. Sarantites, P.F. Hua, M. Devlin et al., “The Microball” Design, instrumentation and response characteristics of a  $4\pi$ -multidetector exit channel-selection device for spectroscopic and reaction mechanism studies with Gammasphere. Nucl. Instrum. Methods Phys. A **381**, 418-432 (1996). <https://doi.org/10.1103/PhysRevC.104.044314>
- [5] J. Gál, G. Hegyesi, J. Molnár et al., The VXi electronics of the DIAMANT particle detector array. Nucl. Instrum. Methods Phys. A **516**, 502-510 (2004). <https://doi.org/10.1016/j.nima.2003.08.158>
- [6] M.J. Koskelo, I.J. Koskelo, B. Sielaff, Comparison of analog and digital signal processing systems using pulsers. Nucl. Instrum. Methods Phys. A **422**, 373-378 (1999). [https://doi.org/10.1016/S0168-9002\(98\)00986-3](https://doi.org/10.1016/S0168-9002(98)00986-3)
- [7] Di-Wen Luo, Hong-Yi Wu, Zhi-Huan Li et al., Performance of digital data acquisition system in  $\gamma$ -ray spectroscopy. Nucl. Sci. Tech. **32**, 79 (2021). <https://doi.org/10.1007/s41365-021-00917-8>
- [8] S. Mitra, L. Wielopolski, G. Hendrey, Comparison of a digital and an analog signal processing system for neutron inelastic  $\gamma$ -ray spectrometry. Nucl. Instrum. Methods Phys. A **61**, 1463-1468 (2004). [https://doi.org/10.1016/S0168-9002\(98\)00986-3](https://doi.org/10.1016/S0168-9002(98)00986-3)
- [9] Chang-lin Lan, Xi-chao Ruan, Gang Liu et al., Particle identification using CsI(Tl) crystal with three different methods. Nucl. Sci. Tech. **19**, 354 (2008). [https://doi.org/10.1016/S1001-8042\(09\)60018-X](https://doi.org/10.1016/S1001-8042(09)60018-X)
- [10] R. Grzywacz, Applications of digital pulse processing in nuclear spectroscopy. Nucl. Instrum. Methods Phys. B **204**, 649-659 (2003). [https://doi.org/10.1016/S0168-583X\(02\)02146-8](https://doi.org/10.1016/S0168-583X(02)02146-8)
- [11] M.S. Badawi, S. Noureddine, Y.N. Kopatch et al., Characterization of the efficiency of a cubic NaI detector with rectangular cavity for axially positioned sources. J. Instrum. **15**, P02013 (2020). <https://doi.org/10.1088/1748-0221/15/02/P02013>
- [12] M.S. Badawi, M. Abd-Elzaher, A.A. Thabet et al., An empirical formula to calculate the full energy peak efficiency of scintillation detectors. Appl. Radiat. Isot. **74**, 46-49 (2013). <https://doi.org/10.1016/j.apradiso.2012.12.011>
- [13] M.I. Abbas, M.S. Badawi, I.N. Ruskov et al., Calibration of a single hexagonal NaI(Tl) detector using a new numerical method based on the efficiency transfer method. Nucl. Instrum. Methods Phys. A **771**, 110-114 (2015). <https://doi.org/10.1016/j.nima.2014.10.056>
- [14] J.C.C. van Melle, G.J. van Nieuwenhuizen, R.J. Meijer et al., Pulse shape analysis of CsI(Tl)-PD signals induced by 6–20 MeV  $\alpha$ -particles and protons. Nucl. Instrum. Methods Phys. A **277**, 584-586 (1989). [https://doi.org/10.1016/0168-9002\(89\)90791-2](https://doi.org/10.1016/0168-9002(89)90791-2)
- [15] LIU Shu-Kui, YUE Qian, LIN Shin-Ted et al., Measurement of intrinsic radioactive backgrounds from the  $^{137}\text{Cs}$  and U/Th chains in CsI(Tl) crystals. Chin. Phys. C, **39**, 046002 (2015). <https://doi.org/10.1088/1674-1137/39/4/046002/meta>
- [16] E.V.D. van Loef, P. Dorenbos, C.W.E. van Eijk et al., High-energy-resolution scintillator:  $\text{Ce}^{3+}$  activated  $\text{LaBr}_3$ . Appl. Phys. Lett. **79**, 1573-1575 (2001). <https://doi.org/10.1063/1.1385342>
- [17] Hao Cheng, Bao-Hua Sun, Li-Hua Zhu et al., Intrinsic background radiation of  $\text{LaBr}_3(\text{Ce})$  detector via coincidence measurements and simulations. Nucl. Sci. Tech. **31**, 99 (2020). <https://doi.org/10.1007/s41365-020-00812-8>
- [18] Wei Lu, Lei Wang, Yong Yuan et al., Monte Carlo simulation for performance evaluation of detector model with a monolithic  $\text{LaBr}_3(\text{Ce})$  crystal and SiPM array for  $\gamma$  radiation imaging. Nucl. Sci. Tech. **33**, 107 (2022). <https://doi.org/10.1007/s41365-022-01081-3>
- [19] Shigekazu Usuda, Akira Mihara, Hitoshi Abe, Rise time spectra of  $\alpha$  and  $\beta(\gamma)$  rays from solid and solution sources with several solid scintillators. Nucl. Instrum. Methods Phys. A **321**, 247-253 (1992). [https://doi.org/10.1016/0168-9002\(92\)90396-L](https://doi.org/10.1016/0168-9002(92)90396-L)
- [20] E.V. Sysoeva, V.A. Tarasov, O.V. Zelenskaya et al., The study of  $\alpha/\gamma$  ratio for inorganic scintillation detectors. Nucl. Instrum. Methods Phys. A **414**, 274 (1998). [https://doi.org/10.1016/S0168-9002\(98\)00011-4](https://doi.org/10.1016/S0168-9002(98)00011-4)
- [21] R.H. Bartram, A. Lempicki, Efficiency of electron-hole pair production in scintillators. J. Lumin. **68**, 225-240 (1996). [https://doi.org/10.1016/0022-2313\(96\)00026-9](https://doi.org/10.1016/0022-2313(96)00026-9)
- [22] R.F. Chen, H.S. Xu, R.R. Fan et al., Property measurement of the CsI (Tl) crystal prepared at IMP. Chin. Phys. C **32**, 135 (2008). <https://doi.org/10.1088/1674-1137/32/2/012>
- [23] D.X. Wang, C.J. Lin, L. Yang et al., Compact 16-channel integrated charge-sensitive preamplifier module for silicon strip detectors. Nucl. Sci. Tech. **31**, 48 (2020). <https://doi.org/10.1007/s41365-020-00755-0>
- [24] XIA LLC, <https://www.xia.com/>
- [25] ROOT Data Analysis Framework, <https://root.cern.ch/>
- [26] W. Skulski, M. Momayezi, Particle identification in CsI(Tl) using digital pulse shape analysis. Nucl. Instrum. Methods Phys. A **458**, 759-771 (2001). [https://doi.org/10.1016/S0168-9002\(00\)00938-4](https://doi.org/10.1016/S0168-9002(00)00938-4)
- [27] Y. Kaschuck, B. Esposito, Neutron/ $\gamma$ -ray digital pulse shape discrimination with organic scintillators. Nucl. Instrum. Methods Phys. A **551**, 420-428 (2005). <https://doi.org/10.1016/j.nima.2005.05.071>
- [28] F. Amorini, C. Boiano, G. Cardella et al., Investigation of the dependence of CsI(Tl) scintillation time constants and intensities on particle's energy, charge and mass through direct fitting of digitized waveforms. IEEE Trans. Nucl. Sci. **59**, 1772 (2012). <https://doi.org/10.1109/TNS.2012.2201499>
- [29] M. Bendel, R. Gernhauser, W.F. Henning et al., RPID — A new digital particle identification algorithm for CsI(Tl) scintillators. Eur. Phys. J. A **49**, 69 (2013). <https://doi.org/10.1140/epja/i2013-13069-8>
- [30] M. Moszyński, D. Wolski, T. Ludziejewski et al., Particle identification by digital charge comparison method applied to CsI(Tl) crystal coupled to photodiode. Nucl. Instrum. Methods Phys. A **336**, 587-590 (1993). [https://doi.org/10.1016/0168-9002\(93\)91267-Q](https://doi.org/10.1016/0168-9002(93)91267-Q)
- [31] Zhuo Zuo, Hao-Ran Liu, Yu-Cheng Yan, et al., Adaptability of n- $\gamma$  discrimination and filtering methods based on plastic scintillation. Nucl. Sci. Tech. A **32**, 28 (2021). <https://doi.org/10.1007/s41365-021-00917-8>
- [32] F. Benrachi, B. Chambon, B. Cheynis et al., Investigation of the performance of CsI(Tl) for charged particle identification by pulse-shape analysis. Nucl. Instrum. Methods Phys. A **281**, 137-142 (1989). [https://doi.org/10.1016/0168-9002\(89\)91225-](https://doi.org/10.1016/0168-9002(89)91225-)

- 4
- [33] J. Williams, C. Andreoiu, G.C. Ball et al., The CsI ball ancillary detector array for TIP and TIGRESS at TRIUMF. Nucl. Instrum. Methods Phys. A **939**, 1-9 (2019). <https://doi.org/10.1016/j.nima.2019.05.069>
- [34] R.A. Bark, M. Lipoglavšek, S.M. Maliage et al., Aspects of nuclear physics research at iThemba LABS, South Africa. J. Phys. G **31**, S1747 (2005). <https://doi.org/10.1088/0954-3899/31/10/066/>
- [35] A. Gavron, Statistical model calculations in heavy ion reactions. Phys. Rev. C **21**, 230 (1980). <https://doi.org/10.1103/PhysRevC.21.230>
- [36] O. Tarasov, D. Bazin, LISE++: Radioactive beam production with in-flight separators. Nucl. Instrum. Methods Phys. B **226**, 4657-4664 (2008). <https://doi.org/10.1016/j.nimb.2008.05.110>
- [37] R. Palit, H.C. Jain, P.K. Joshi et al., Shape coexistence in  $^{72}\text{Se}$ . Phys. Rev. C **63**, 024313 (2001). <https://doi.org/10.1103/PhysRevC.63.024313>
- [38] J. Döring, G.D. Johns, M.A. Riley et al., Band structures and alignment properties in  $^{74}\text{Se}$ . Phys. Rev. C **57**, 6 (1998). <https://doi.org/10.1103/PhysRevC.57.2912>
- [39] F.G.A. Quarati, P. Dorenbos, J.van der Biezen et al., Scintillation and detection characteristics of high-sensitivity  $\text{CeBr}_3$  gamma-ray spectrometers. Nucl. Instrum. Methods Phys. A **719**, 596-604 (2013). <https://doi.org/10.1016/j.nima.2013.08.005>
- [40] J.M. Regis, G.S. Simpson, A. Blanc et al., Germanium-gated  $\gamma$ - $\gamma$  fast timing of excited states in fission fragments using the EXILL&FATIMA spectrometer. Nucl. Instrum. Methods Phys. A **763**, 210-220 (2014). <https://doi.org/10.1016/j.nima.2014.06.004>
- [41] D. Bucurescu, I.Cata-Danil, G. Ciocan et al., The ROSPHERE  $\gamma$ -ray spectroscopy array. Nucl. Instrum. Methods Phys. A **837**, 1-10 (2016). <https://doi.org/10.1016/j.nima.2016.08.052>
- [42] C. Mihai, A.A. Pasternak, D. Filipescu et al., Side feeding patterns and nuclear lifetime determinations by the Doppler shift attenuation method in  $(\alpha, n\gamma)$  reactions. Phys. Rev. C **81**, 034314 (2010). <https://doi.org/10.1103/PhysRevC.81.034314>
- [43] A. Dewald, S. Harissopulos, P. von Brentano, The differential plunger and the differential decay curve method for the analysis of recoil distance Doppler-shift data. Z. Phys. A **334**, 163-175 (1989). <https://doi.org/10.1007/BF01294217>
- [44] N. Marginean, D.L. Balabanski, D. Bucurescu et al., Tin-beam measurements of sub-nanosecond nuclear lifetimes with a mixed array of HPGe and  $\text{LaBr}_3:\text{Ce}$  detectors. Eur. Phys. J. A **46**, 329-336 (2010). <https://doi.org/10.1140/epja/i2010-11052-7>
- [45] T. Teranishi, Y. Ueno, M. Osada et al., Pulse shape analysis of signals from SiPM-based CsI(Tl) detectors for low-energy protons: Saturation correction and particle identification. Nucl. Instrum. Methods Phys. A **989**, 164967 (2021). <https://doi.org/10.1016/j.nima.2020.164967>
- [46] Yu Sun, Zhi-Yu Sun, Yu-Hong Yu et al., Temperature dependence of CsI:Tl coupled to a PIN photodiode and a silicon photomultiplier. Nucl. Sci. Tech. **30** 27 (2019). <https://doi.org/10.1007/s41365-019-0551-0>